Statistical Estimation of Operating Reserve Requirements using Rolling Horizon Stochastic Optimization

Site Wang[1], Harsha Gangammanavar*[2], Sandra Ekşioğlu[1], and Scott Mason[1]

[1]Department of Industrial Engineering, Clemson University, Clemson, SC
[2]Department of Engineering Management, Information, and Systems, Southern Methodist University, Dallas TX

Current version: 11/2019 (First submission: 09/2016)

Abstract

We develop a multi-period stochastic optimization framework for identifying operating reserve requirements in power systems with significant penetration of renewable energy resources. Our model captures different types of operating reserves, uncertainty in renewable energy generation and demand, and differences in generator operation time scales. Along with planning for reserve capacity, our model is designed to provide recommendations about base-load generation in a non-anticipative manner, while power network and reserve utilization decisions are made in an adaptive manner. We propose a rolling horizon framework with look-ahead approximation in which the optimization problem can be written as a two-stage stochastic linear program (2-SLP) in each time period. Our 2-SLPs are solved using a sequential sampling method, stochastic decomposition, which has been shown to be effective for power system optimization. Further, as market operations impose strict time requirements for providing dispatch decisions, we propose a warm-starting mechanism to speed up this algorithm. Our experimental results, based on IEEE test systems, establish the value of our stochastic approach when compared both to deterministic rules from the literature and to current practice. The resulting computational improvements demonstrate the applicability of our approach to real power systems.

1 Introduction

Renewable energy resources are critical for the future of power grids. These sustainable and clean energy resources have the potential of addressing global warming concerns and improving environmental quality. However, some renewable energy resources, like wind and solar, introduce high degree of variability and uncertainty in the operations of power systems. Currently, independent system operators (ISO) use deterministic frameworks that use a single forecast of uncertainty as system input. This practice's effectiveness largely depends on the accuracy of the forecast, which is particularly hard to achieve for intermittent resources. According to Price (2015), as modeling uncertainty inherent in renewable energy generation is critical for maintaining robust power systems, frameworks that treat uncertainty using simple statistical or probabilistic measures may misrepresent the benefits that could be provided by them. (Sen et al., 2006) indicate stochastic frameworks might be able to address intermittency more effectively and provide higher quality solutions.

Power systems implement a hierarchical balancing process that mainly includes day-ahead unit commitment (DA-UC), short-term unit commitments (ST-UC), and economic dispatch

*harsha@smu.edu

(ED) (e.g., see (Atakan et al., 2019) for detailed discussion). These processes use information of incremental accuracy. In any case, there may be discrepancies between planned resources and actual utilization. Fast-ramping operating reserves play a critical role in addressing such energy imbalances. Large-scale introduction of intermittent resources has inevitably introduced a new degree of dispatchability issues for operating reserves. Moreover, the level of operating reserves is not constant during all hours of a day. This necessitates tools that dynamically identify the reserve requirements based on the nature of underlying stochastic processes. According to (Olson et al., 2015), failure to accommodate these challenges will result in over-generation of energy and an increased need for ramping capability.

Determination of reserve requirements (RR) has attracted significant attention in recent years. The early systems used to set the requirements to be greater than or equal to the capacity of the largest online generator. More recently, system operators use deterministic policies, which are in part based on statistical variation in renewable energy generation and demand. For example, in the Electric Reliability Council of Texas (ERCOT) region, the requirements are set to the 98.8th percentile of reserves utilized in the previous 30 days and in the same month of last year Erik et al. (Aug. 2011). Other approaches use more advanced probabilistic metrics such as loss of load probability (Chattopadhyay and Baldick (2002)), expected load not served (Bouffard and Galiana (2004)), and expected energy not supplied (Ortega-Vazquez and Kirschen (2009)). However, computing the desired reliability metric in this manner requires simplifying assumptions on underlying probability for renewable energy generation and demand distributions (such as normal error on net-demand).

Stochastic programming (SP) approaches have been used in a combined UC-ED models to identify commitment (procurement) decisions for operating reserves (e.g., (Zheng et al., 2015) and (Papavasiliou et al., 2011)). These UC-ED formulations, which turn out to be mixed-integer SP models, often exclude transmission constraints in their models to attain computational tractability. A common practice is to use relaxations that use aggregated stochastic processes where the total net demand is set equal to the total generation. Programs driven by such aggregations result in optimal decisions with little room for error when implemented. Since network topology is ignored in such relaxations, the solutions obtained over-estimate the capability of the system to deliver reserves, and therefore, the estimated reserve requirements fall short of what actually is needed. Models which incorporate transmission network have also been proposed. A UC formulation was proposed to identify geographical allocations of the reserve in an interconnected multi-area power system in (Ahmadi-Khatir et al., 2014). The problem is solved using a decentralized algorithm based on an augmented Lagrangian method. In this case, computational tractability was achieved by considering a limited number of scenarios (10 wind power scenarios). Use of such limited scenarios misrepresents the uncertainty inherent in the system. This is particularly true in power systems with significant renewable penetration as stated in (Gangammanavar et al., 2016). Therefore, the reserve requirements estimated using approaches based on a small number of scenarios can again be misleading. A simulation based approach provides a systematic tool to overcome the biased estimates of limited scenarios. Such an approach was employed in the case study on penetration of renewable resources in the state of California in (Olson et al., 2015). However, a setting based just on simulation ignores the system operational restrictions such as the non-anticipative nature of certain decisions and the possibility of taking adaptive recourse actions.

In our paper, we propose a novel modeling and algorithmic framework to estimate reserve requirements considering uncertainty in renewable generation and demand. As opposed to methods based on probabilistic measures (Erik et al. (Aug. 2011), Chattopadhyay and Baldick (2002), Bouffard and Galiana (2004), and Ortega-Vazquez and Kirschen (2009)), UC-ED simulation-based methods (Olson et al. (2015)), and UC-ED optimization-based methods (Papavasiliou et al. (2011), Zheng et al. (2015), and Ahmadi-Khatir et al. (2014)), our method is based on a rolling horizon ED setup. The operating reserves requirements are estimated using a com-

bination of optimization and simulation. Our model incorporates the power flow equations to capture the network restrictions that effect the reserve requirement estimation. Our algorithm utilizes sequential sampling techniques to efficiently estimate system uncertainty. Such techniques incorporate simulation while the optimization process is being carried out. It constantly tracks the response of optimization to an ever-increasing set of scenarios without compromising on computational tractability. We would like to emphasize that unlike the UC-ED methods where the goal is to identify reserve commitment decisions, our goal is to obtain a statistical estimate of reserve requirements. The reserve requirements concluded here serve as assertive information for scheduling problems, such as DA-UC and ST-UC. Using these estimates, the UC problem can then effectively schedule the generators by enforcing the traditional operational requirements (up/down-time, etc.).

In light of this, the main contributions of our work are:

1. A *decision model* that includes different types of operating reserves (following, regulating, and ramping), power flow equations, uncertainty in renewable energy generation and demand, and differences in operating time scales of generators in the system. Our model allows a certain fraction of each reserve's capacity to be allocated for regulating service ahead of time in order to address future power imbalances. The model is a multi-period stochastic program that can be decomposed into computationally-viable, two-stage stochastic linear programs (2-SLPs) at each time period. These 2-SLPs are linked by linear dynamics and a look-ahead approximation. The model, which is presented in §2, allows the combination of statistical estimation and optimization of reserve requirements that can then be enforced by the ISO in a traditional UC problem with pool-based market constraints (for example, (Motto et al., 2002)).

2. A *stochastic framework* that combines optimization and simulation in a rolling horizon setting (presented in §3). This framework addresses the short-comings of deterministic and probabilistic policies, and incorporates simulations within optimization. Determining operating reserves by simulation alone is an anticipative approach, in which the reserve planning decisions are made in response to a simulated scenario. In practice, however, these decisions are required to be made before such a realization is available. By combining optimization and simulation, our framework not only provides optimal non-anticipative reserve planning decisions, but it also provides statistical guarantees on them. This is achieved by incorporating two-stage stochastic decomposition (SD) as the optimization engine and a novel warm-starting scheme to address computational time requirements.

3. Designed *computational experiments* that are conducted on instances created using IEEE test system data (118 and 300) and Western Wind and Solar Integration Study (WWSIS) renewable energy generation datasets. These experiments indicate the advantages of our stochastic framework over deterministic approaches both in terms of solution quality as well as objective value estimates. Furthermore, our results demonstrate the computational efficiency and scalability achieved by using the proposed warm-starting scheme. These results are presented and discussed in §4.

2 Decision Model

We consider a multi-period stochastic reserve requirement model (MS-RR) that aims to minimize the total expected operating cost over a finite horizon. The system is comprised of energy resources that include slow ramping conventional generators, operating reserves, and renewable generators. These resources are used to meet the system demand while satisfying power network constraints. In this section, we will present a SP formulation of this problem. For ease of reading, we have provided the list of notations in Appendix-B.

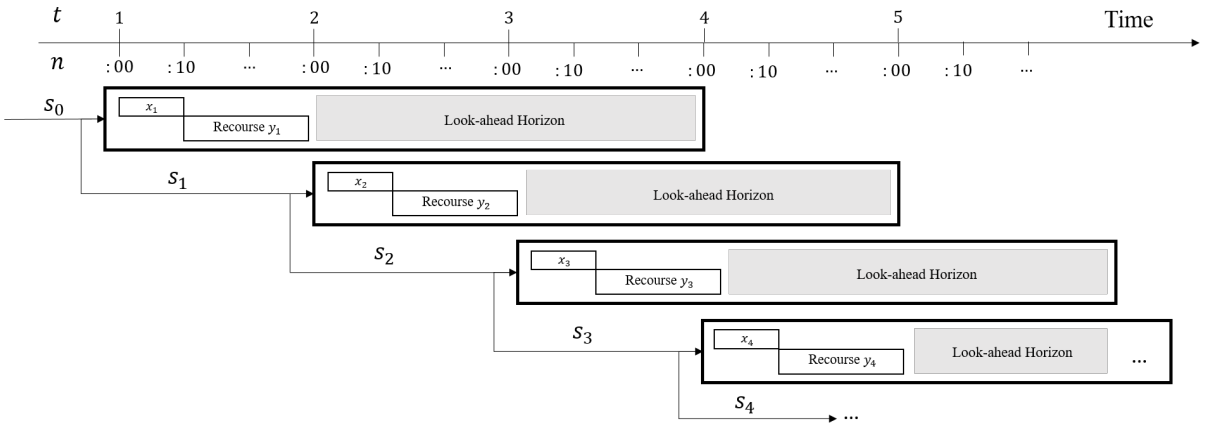

Figure 1: One-hour Decision Frequency with 10-minute Model Resolution and 2-hour Maximum Look-head Horizon

Decision Timeline

The reserve requirement problems are solved periodically (every few minutes) over a certain horizon where generation unit commitments are fixed in (Makarov et al., 2010). These periodic decision epochs are denoted by $\mathcal{T} := \{1 \cdots T\}$. In practice, this decision frequency ranges from 5-10 minutes to a few hours. At each $t \in \mathcal{T}$, decisions can be categorized into two sets: those made before the realization of uncertainty, and those made after. The former, which includes certain conventional generation levels, operating reserve requirements, etc., will be referred to as the first-stage (or here-and-now) decisions and denoted by x_t. In response to these decisions and a realization (b_t) of the random variable ($\tilde{\omega}_t$), certain recourse actions related to network flows, operating reserves, renewable energy generation, etc., can be made. These recourse actions are taken at fine time scale denoted by $n \in \mathcal{N} := \{1 \cdots N\}$, whose range is from 5-10 minutes. While $t \in \mathcal{T}$ is related to the frequency at which x_t are made, the $n \in \mathcal{N}$ captures the model resolution. In the case of certain system operators (CAISO), both decision frequency and model resolution are equal (5 minutes). When using SP models on the other hand, Gangammanavar et al. (2016) recommend that decisions be made every hour using models with a 20 minute resolution for their test instances that including those for a power system for the state of Illinois. The recourse decisions are referred to as the second-stage (or anticipative) decisions and are denoted as $y_t(\omega_t)$. For brevity, the dependence of second stage decisions on (ω_t) is omitted and represented simply as y_t. The random variable $\tilde{\omega}_t$ captures uncertainty in renewable generation and demand. The decision timeline adopted in this paper is shown in Figure. 1. We begin our model presentation by discussing different energy resources.

2.1 Base-Load Generators

Base-load generators, denoted by the set $\mathcal{G}^B$, are large generation capacity units that meet the majority of system demand. However, they are physically limited by their ramp rates, and therefore, their generation levels $(x^b_{ti})_{i \in \mathcal{G}^B}$ need to be decided ahead, at time periods $t \in \mathcal{T}$. These decisions are constrained by the following capacity and ramping limits:

$$G_i^{b,min} \leq x^b_{ti} \leq G_i^{b,max}, \tag{1a}$$

$$\Delta G_i^{b,min} \leq x^b_{ti} - x^b_{t-1,i} \leq \Delta G_i^{b,max}, \qquad \forall i \in \mathcal{G}^B. \tag{1b}$$

2.2 Operating Reserves

Power systems deploy operating reserves to resolve variability and uncertainty. These reserves provide additional generation capacity for assistance in power balancing. The categorization of operating reserves has different terminologies and definitions over different regions. In our model, we consider three types of operating reserves: following reserves, regulating reserves, and ramping reserves. Our terminology and definition of these reserve types follows their usage in (Erik et al., Aug. 2011) (see Table I of the report).

2.2.1 Following Reserves

The following reserves are also referred to as the load following, schedule, dispatch and balancing reserves. These reserves utilize forecast load and renewable energy generation to correct energy imbalances that are expected to occur. Since their operation is based on forecast information, these decisions are made at every $t \in \mathcal{T}$ along with base-load generators. Further, they are more flexible than base-load generators, and hence the generation levels can fluctuate at a fine time scale (i.e. at $n \in \mathcal{N}$). With $\mathcal{G}^F$ as the set of these reserves, their generation $(x^f_{tni})_{i\in\mathcal{G}^F}$ at every fine time period $n \in \mathcal{N}$ (within each period t) are constrained by:

$$G_i^{f,min} \leq x^f_{tni} \leq G_i^{f,max}, \tag{2a}$$

$$\Delta G_i^{f,min} \leq x^f_{tni} - x^f_{t,n-1,i} \leq \Delta G_i^{f,max}, \qquad \forall i \in \mathcal{G}^F. \tag{2b}$$

2.2.2 Regulating Reserves

These reserves have faster ramp-rates than the following reserves, and can be controlled at fine time periods, and are sometimes referred to as secondary control. While following reserves are established based on forecast information, regulating reserve utilization depends on actual realization of uncertain parameters. Such regulating services are provided by certain spinning generation units, which are denoted by $\mathcal{G}^S$. These generators can be dispatched along with base-load generators at $t \in \mathcal{T}$. In addition to the up-front dispatch, a certain fraction of generator capacity is devoted to provide both regulation-up and -down services in the future. The up-front dispatch is denoted as $x^s_{ti} \in \mathbb{R}^+$, while the capacity for regulation-up and -down are denoted as $x^{p+}_{ti} \in \mathbb{R}^+$, and $x^{p-}_{ti} \in \mathbb{R}^+$, respectively. These quantities together must satisfy:

$$G_i^{s,min} \leq x^s_{ti} + x^{p+}_{ti} - x^{p-}_{ti} \leq G_i^{s,max} \quad \forall i \in \mathcal{G}^S. \tag{3}$$

As with base-load and following reserve generation levels, the up-front dispatch and estimated future reserve requirements of spinning generators are elements of first-stage decisions. We use the decision vector

$$x_t = [(x^b_{ti})_{i\in\mathcal{G}^B}, (x^f_{ti})_{i\in\mathcal{G}^F}, (x^s_{ti})_{i\in\mathcal{G}^S}, (x^{p+}_{ti})_{i\in\mathcal{G}^S}, (x^{p-}_{ti})_{i\in\mathcal{G}^S}]$$

to denote the consolidated first-stage decisions.

The actual fraction of reserves utilized in correcting system imbalances, however, depends on the realization of demand and renewable energy generation at each fine time period $n \in \mathcal{N}$. Therefore, the utilization decisions $u^s_{tni} \in \mathbb{R}$ are considered to be second-stage decisions. These regulating reserves are constrained by their ramping limits. Such constraints are applicable to the actual generation of regulating reserves $i \in \mathcal{G}^S$, i.e., $x^s_{ti} + u^s_{tni}$, and are given for all $t \in \mathcal{T}$ by:

$$\Delta G_i^{s,min} \leq x^s_{ti} + u^s_{t1i} - x^s_{t-1,i} - u^s_{t-1,N,i} \leq \Delta G_i^{s,max}, \tag{4a}$$

$$\Delta G_i^{s,min} \leq u^s_{tni} - u^s_{t,n-1,i} \leq \Delta G_i^{s,max}, \forall n \in \mathcal{N} \setminus \{1\}. \tag{4b}$$

Note that the actual overall generation level at the beginning of time period t depends on the terminal state of time period $(t-1)$, which in turn depends on the realization encountered. This is captured in (4). Finally, it is expected that the utilization of these reserves does not exceed the estimated regulating reserve capacity:

$$-x^{p-}_{ti} \leq u^s_{tni} \leq x^{p+}_{ti}, \quad n \in \mathcal{N}, t \in \mathcal{T}. \tag{5}$$

Realistically, the up-front dispatch cost of these resources, which is denoted by c^s_i, is lower than the cost associated with utilizing these resources as spinning reserves. The cost associated with planning regulation-up reserves is denoted as c^p_i, while utilizing these resources will cost an additional d^s_i units. These costs satisfy $c^s_i \leq c^p_i + d^s_i$. We assume that the planning cost associated with regulation-down reserves is also c^p_i, and there is no additional cost of utilizing this services.

2.2.3 Ramping Reserves

Due to greater uncertainty of renewable resources, infrequent large magnitude events may occur that require reserves beyond that which can be provided by the following and regulating reserves. Ramping reserves serve as the last line of resources to overcome such system imbalances. Therefore, their generation decisions are naturally anticipative and are the most expensive set of resources. Let $\mathcal{G}^R$ be the set of ramping reserves and let $(u^r_{tni})_{i\in\mathcal{G}^R} \in \mathbb{R}$ denote the corresponding capacity provided during fine time period n at the cost of d^r_i ($d^r_i \gg c^s_i + c^p_i$). Their usage is reflected through the power flow equation that we describe later in the section.

Establishing the appropriate requirements of regulating reserves ($i \in \mathcal{G}^S$) is critical to lower the overall operating cost. Note that these are the first stage decisions. If excess amount is scheduled, these resources may be left under-utilized. On the other hand, scheduling an insufficient amount of spinning reserves will result in an increased usage of the more expensive ramping reserves. Either of these cases drives the operating cost higher.

In the first-stage, the best available information regarding demand and renewable energy generation are their point forecasts. Therefore, the first-stage generation decisions are tied by the following constraint at each $n \in \mathcal{N}$:

$$\sum_{i\in\mathcal{G}^F} x^f_{tni} + \sum_{i\in\mathcal{G}^B} x^g_{ti} + \sum_{i\in\mathcal{G}^S} x^s_{ti} \geq \Delta\widehat{L}_{tn}, \tag{6}$$

where $\Delta\widehat{L}_{tn}$ is the system-wide forecasted net-demand. This quantity is computed as the total forecasted demand minus the total forecasted renewable generation, i.e., $\Delta\widehat{L}_{tn} := \sum_{i\in\mathcal{D}} \widehat{L}_{tni} - \sum_{i\in\mathcal{W}} \widehat{W}_{tni}$. Note that the first-stage decisions serve as a directive for planning and are not the actual generation amounts. Therefore, we only make sure that the planned resources exceed the best available forecast at the time of planning.

2.3 Power Network

To ensure that demand at every bus is fulfilled by available resources, while ensuring that the physical limitations of the network are satisfied, we consider a detailed power network model, where $\mathcal{B}$ denotes the set of buses and $\mathcal{L}$ the set of transmission lines.

In our model, we consider a linear approximation of AC power flow as in (Motto et al., 2002), and ignore power losses. If V_i denotes voltage of bus i and X_{ij} the reactance of line $(i,j) \in \mathcal{L}$, then the power flow p_{tnij} on any line (i,j) is given by:

$$p_{tnij} = \frac{V_i V_j}{X_{ij}}(\theta_{tni} - \theta_{tnj}) \quad \forall n \in \mathcal{N}, t \in \mathcal{T}, \tag{7}$$

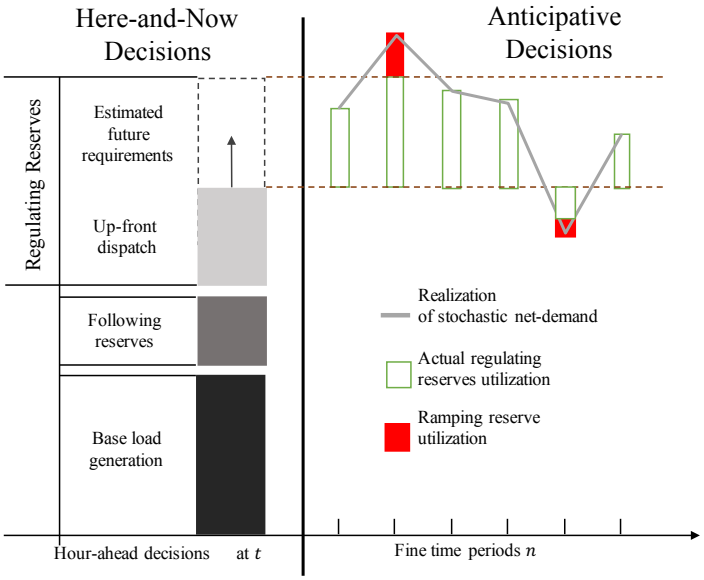

Figure 2: Generation Composition and Decision Structure

where θ_{tni} is a decision variable of bus voltage angle. Moreover, the decisions p_{tnij} and θ_{tni} are required to be within intervals $[p^{min}, p^{max}]$ and $[\theta^{min}, \theta^{max}]$, respectively.

At any node, the total available power should be equal to the demand at that node. This is guaranteed at every bus $i \in \mathcal{B}$ and fine time period $n \in \mathcal{N}$ by the following flow balance equation:

$$\sum_{j:(j,i)\in\mathcal{L}} p_{tnji} - \sum_{j:(i,j)\in\mathcal{L}} p_{tnij} + \sum_{j\in\mathcal{G}_i^S} u^s_{tnj} + \sum_{j\in\mathcal{D}_i} u^r_{tnj} = \sum_{j\in\mathcal{D}_i\cup\mathcal{W}_i} \Delta\widetilde{L}_{tnj} - \left(\sum_{j\in\mathcal{G}_i^B} x^b_{tj} + \sum_{j\in\mathcal{G}_i^S} x^s_{tj} + \sum_{j\in\mathcal{G}_i^F} x^f_{tnj} \right). \tag{8}$$

Here, $\Delta\widetilde{L}_{tnj}$ is the net-demand which is defined as the difference between the actual demand and renewable generation:

$$\Delta\widetilde{L}_{tni} = \sum_{j\in\mathcal{D}_i} \widetilde{L}_{tnj} - \sum_{j\in\mathcal{W}_i} \widetilde{W}_{tnj} \quad i \in \mathcal{B}. \tag{9}$$

We model the actual demand and renewable generation as random variables $\tilde{L}_{tni}$ for all $i \in \mathcal{D}$ and $\widetilde{W}_{tni}$ for all $i \in \mathcal{W}$, respectively. This implies that net-demand $\Delta\widetilde{L}_{tni}$ is also a random quantity[1]. With this, the left-hand side of the equation (8) captures the total available power at bus i that includes the power flows into/out of the bus, the actual utilization of regulating reserves and the utilization of ramping reserves. The parenthetical term on the right-hand side represents the first-stage generation levels at bus i. Notice that the decision variables on the left-hand side of equation (8) depend on the realized scenario, and therefore, are anticipative in nature. These are summarized using the vector

$$y_t = ((p_{tnij})_{(i,j)\in\mathcal{L}}, (\theta_{tni})_{i\in\mathcal{B}}, (u^s_{tni})_{i\in\mathcal{G}^S}, (u^r_{tni})_{i\in\mathcal{G}^R})_{n\in\mathcal{N}},$$

and constitute the second-stage decisions.

[1]This is in contrast to the forecasted net-demand $\widehat{L}_{tn}$ that appears in (6) which is a deterministic quantity.

2.4 Objective Function

Following the categorization of decision variables, the objective at every time period $t \in \mathcal{T}$ also comprises of two parts: the first corresponds to the here-and-now decisions, and the second is the recourse cost. The here-and-now costs include the generation costs associated with the base-load generators $\mathcal{G}^B$, up-front dispatch and planned regulation up/down costs for regulating reserves $\mathcal{G}^S$, and costs associated with following reserves $\mathcal{G}^F$. These are captured by

$$f(x_t) := \sum_{i \in \mathcal{G}^B} c_i^b x_{ti}^b + \sum_{i \in \mathcal{G}^S} (c_i^s x_{ti}^s + c_i^p x_{ti}^{p+} + c_i^p x_{ti}^{p-}) + \sum_{n \in \mathcal{N}} \sum_{i \in \mathcal{G}^F} c_i^f x_{tni}^f. \tag{10}$$

The recourse cost for a particular realization ω_t captures the cost of utilizing regulating and ramping reserves which is given as:

$$g(y_t) = \sum_{n \in \mathcal{N}} \left[\sum_{i \in \mathcal{G}^S} d_i^s (u_{tni}^s)_+ + \sum_{i \in \mathcal{D}} d_i^r u_{tni}^r \right]. \tag{11}$$

Here $(u)_+ = \max[0, u]$ captures the non-negative utilization of regulating-up reserves. Notice that both the here-and-now and recourse costs are affine functions of their respective decision vectors which can succinctly be written as $f(x_t) = c^\top x_t$ and $g(y_t) = d^\top y_t$, respectively.

2.5 Stochastic Processes

To facilitate the description of the underlying stochastic process, we consider a time index τ for fine time periods $n \in \mathcal{N}$ which captures the elapsed time from the beginning. For example, the fine time periods in coarse interval t are indexed as $\tau = N(t-1), N(t-1)+1, \ldots, N(t-1)+(N-1)$. With this, the vector $\widetilde{W}_{tn}$ can be written as $\widetilde{W}_\tau$ where $\tau = (t-1) * N + n$.

Statistical models have previously been used to represent renewable energy generation (Morales et al. (2010)) and demand (Sen et al. (2006)). The early works considered separate univariate models for different locations, e.g. (Brown et al., 1984), which were later extended to multivariate models in (Papavasiliou and Oren, 2013). We adopt a similar approach and represent demand and renewable energy generation stochastic processes as multivariate time series, which have the form (shown for renewable energy generation) $\widetilde{W}_\tau = \eta_\tau + \tilde{\omega}_\tau$, where

$$\tilde{\omega}_\tau = \sum_{i=1}^{p} \Phi_i \omega_{\tau-i} + \sum_{i=1}^{q} \Theta_i \epsilon_{\tau-i} + \tilde{\epsilon}_\tau. \tag{12}$$

Here $\{\eta_\tau\}$ is the deterministic component that captures trend and seasonality, and $\{\tilde{\omega}_\tau\}$ is the residual process. For ease of exposition, we assume that the residual time-series is stationary and hence can be modeled as an ARMA(p, q) process as shown in (12), where $\{\tilde{\epsilon}_\tau\}$ follows normal distribution. The principal steps of estimating the coefficients of the ARMA model are discussed in Appendix A and we refer the reader to (Hamilton, 1994) for greater details. Note that the model presented in (12) can be decomposed into deterministic and stochastic components. For example, for $\tau = Nt + n'$, this decomposition yields:

$$\tilde{\omega}_\tau = \left[\sum_{i=1}^{n'} \Phi_i \tilde{\omega}_{\tau-i} + \sum_{i=1}^{n'} \Theta_i \tilde{\epsilon}_{\tau-i} + \tilde{\epsilon}_\tau \right] + \left[\sum_{i=n'+1}^{p} \Phi_i \omega_{\tau-i} + \sum_{i=n'+1}^{q} \Theta_i \epsilon_{\tau-i} \right]. \tag{13}$$

At time period t(i.e., $\tau = Nt \cdots Nt + N$), the term in the first bracket is stochastic as it is computed using residuals and noise from current time period. We denote this term as $\Delta\tilde{\Gamma}_t$. On the other hand, the terms in the second bracket are computed using residuals and noise from the previous time period $t-1$; therefore, they are deterministic. This term is denoted by $\bar{\Gamma}_t$. Finally, we refer the reader to Figure 3 for a demonstration of this stochastic process.

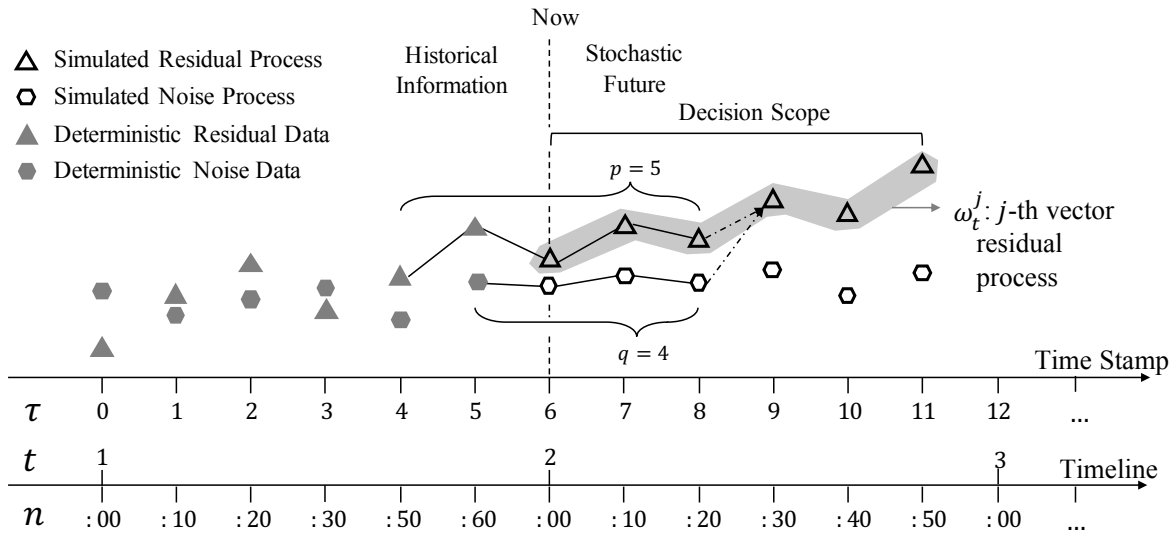

Figure 3: Graphical Representation of Stochastic Processes with Example ARMA$(5, 4)$ and $N = 6$

2.6 Mathematical Structure

To summarize, at each time period $t \in \mathcal{T}$, our MS-RR problem comprises of non-anticipative decisions x_t and recourse decisions $y_t(\omega_t)$. These decisions are made in an uncertain environment captured by the stochastic process given in §2.5. The state of the system at the beginning of time period t is captured by the state variable s_t. We will defer the description of this state variable until later in this section. For a given state s_t, the optimization model can be stated as a 2-SLP which can succinctly be written as:

$$v_t(s_t) = \min \; c^\top x_t + \mathbf{E}\{h_t(s_t, x_t, \tilde{\omega}_t)\} + \ell_t(s_{t+1}) \tag{14a}$$

$$\text{s.t. } x_t \in \mathcal{X}_t(s_t). \tag{14b}$$

Here, the first-stage feasible region $\mathcal{X}_t(s_t)$ is a polyhedron characterized by constraints (1) – (3) and (6).

If optimization at time period t only considers operations at the current time period, then we might end up with myopic decisions. This in turn may result in infeasibility or higher operating costs in future time periods. On the other hand, treating the future time periods at the same level of detail as the current time period will result a computationally unwieldy model, particularly for real-scale systems. Therefore, we follow the approach suggested by (Zavala, 2016) and (Dvorkin et al., 2015) and include a look-ahead approximation in the first-stage. This look-ahead approximation captures the operations over the future time periods ($t' = t+1, \ldots, T$) only along the point forecast, and at a lower resolution. In our experiments we consider look-ahead decisions only at the course timescale. In this case, the cost the look-ahead horizon is captured by the function $\ell_t(s_{t+1}) = \sum_{t'=t+1}^{T} f(x_{t'})$. The description of the feasible region $\mathcal{X}_t(s_t)$ additionally includes constraints (1), (2)[2] , (3) and (6) for time periods $t' = t+1, \ldots, T$.

For a given first-stage decision x_t and a realization ω_t of the stochastic process $\tilde{\omega}_t$, the

[2]The ramping constraints in (2b) are written for the fine timescale of the model. For the look-ahead time periods, these constraints need to be modified to reflect ramp limits over the look-ahead resolution. For example, when the look-ahead resolution is the same as coarse timescale, the ramp-up and ramp-down limits will be $N \times \Delta G_i^{f,max}$ and $N \times \Delta G_i^{f,min}$, respectively.

recourse function is given by:

$$h_t(s_t, x_t, \omega_t) = \min\ d^\top y_t(\omega_t) \tag{15a}$$

$$\text{s.t. } y_t(\omega_t) \in \{y \mid Dy_t = b_t(s_t, \omega_t) - C_t x_t\}. \tag{15b}$$

The second-stage feasible region in (15b) is also a polyhedron defined by (4)–(5) and (7)–(9).

Notice that the ramping constraints for base-load, following reserves and regulating reserves ((1b), (2b) and (4b), respectively) depend on both the first-stage and second-stage decisions of previous time period. If the first-stage decision is x_{t-1} and the actual realization of the stochastic process is denoted by $\bar{\omega}_{t-1}$, then we can use (15) to identify the second-stage decision $y_{t-1}(\bar{\omega}_{t-1})$. Further, the deterministic component η_t is necessary to simulate scenarios of the stochastic process. In order to capture these, our description of the state variable comprises of three components: the first-stage decision x_{t-1} for time period $t-1$, and the second-stage decision $y_{t-1}(\bar{\omega}_{t-1})$ corresponding to the actual realization of the stochastic process in time period $t-1$, and the deterministic component η_t of the stochastic process for time period t, i.e., $s_t := (x_{t-1}, y_{t-1}(\bar{\omega}_{t-1}), \eta_t)$.

Before we close this section, we note that the right-hand side $b_t(s_t, \tilde{\omega}_t)$ in (15b) is a consolidated vector of the right-hand sides of all constraints and can be written as:

$$b_t(s_t, \tilde{\omega}_t) = \bar{b}_t(s_t, \bar{\Gamma}_t) + \Delta b_t(\Delta\tilde{\Gamma}_t). \tag{16}$$

The above representation follows from the decomposed representation of the stochastic process in equation (13), and plays a critical role in the design of our computer implementation.

3 Algorithm

In this section, we introduce a rolling horizon, stochastic programming algorithm to tackle the formulation in §II. We use stochastic decomposition (SD), a sequential sampling algorithm, to optimizing the 2-SLP at each time period $t \in \mathcal{T}$. The difficulty associated with optimizing a 2-SLP centers around the computation of the expectation in (14a). The classical algorithms designed to address 2-SLPs include cutting-plane/outer-linearization methods, such as the L-shaped method (Van Slyke and Wets (1969)) and their many extensions, inner-linearization methods based on Dantzig-Wolfe decomposition (Dantzig and Wolfe (1960)), and scenario decomposition methods such as progressive hedging (Rockafellar and Wets (1991)). These algorithms were designed to solve 2-SLPs with a finite discrete distribution. When the probability distribution is continuous, sampling-based techniques typically are employed to generate a set of scenario. These random scenarios are either based on historical data, or are generated using Monte Carlo sampling techniques. This leads to a sample average approximation (SAA) of the expected recourse function:

$$\mathbf{E}\{h_t(s_t, x_t, \tilde{\omega}_t)\} \sim \frac{1}{S}\sum_{i=1}^{S} h_t(s_t, x_t, \hat{\omega}_t^i). \tag{17}$$

The choice of S plays a critical role in determining the accuracy of SAA, and hence, the quality of solution obtained. SAA is an unbiased estimator of the objective function and converges uniformly to the true expectation function as the number of scenarios increases (Shapiro et al. (2014)). However, if S is found to be inadequate, the objective function estimates are known to be negatively biased. The computational requirements for solving an optimization problem having a large S is very high. This limits its tractability for large-scale applications such as the one considered in our study.

If SAA is employed, the process begins by searching a scenario size, simulating the scenarios, and then optimizing the problem for simulated scenarios (Linderoth et al. (2006)). The process

continues until satisfactory performance, measured in terms of the optimality gap computed using upper and lower bound estimates, is obtained. When performance is unsatisfactory, the sample size is increased, a new set of scenarios with larger S is generated, and the corresponding optimization models are solved. Unfortunately, the time required to obtain a solution using SAA often exceeds the strict solution time restrictions in power system operations.

The sequential sampling approach employed in SD is designed to address this shortcoming. We extend SD to a rolling-horizon setting suitable for our application. Motivated by the structure of the stochastic process described in §2.5, a warm-starting mechanism is introduced. We first present a brief summary of the SD algorithm, followed by our proposed enhancements. As our 2-SLP model satisfies fixed and relatively complete recourse properties (Birge and Louveaux (2011)), we present our algorithm under these assumptions.

3.1 Stochastic Decomposition

In this subsection, we introduce the SD algorithm presented in Algorithm 1. Conceptually, SD is a stochastic counterpart to the L-shaped method where the affine lower bounds computed in each iteration are stochastic in nature. It uses sequential sampling to build an incremental sample average of the expected recourse function. In iteration k this is given as:

$$\mathbf{E}\{h_t(s_t, x_t, \tilde{\omega}_t)\} \sim H_t^k(s_t, x_t) := \frac{1}{k}\sum_{i=1}^{k} h_t(s_t, x_t, \hat{\omega}_t^i). \tag{18}$$

This approximation is updated by introducing a new scenario in every iteration (there are k scenarios in iteration k, as opposed to a fixed S in (17)).

Consider the principal steps of SD in iteration k. At the beginning of this iteration, we have first-stage solution x_t^k and certain approximation $f_t^{k-1}(s_t, x_t)$. A new scenario $\omega_t^k = (\omega_{tn}^k)_{\forall n \in \mathcal{N}}$ is incorporated into a collection of existing outcomes, $\Omega := \{\omega_t^1, \omega_t^2, \cdots, \omega_t^{k-1}\}$ (Step 5). For the most recent scenario ω_t^k and first-stage decision x_t^k, we evaluate a recourse function by solving $h_t(s_t, x_t^k, \omega_t^k)$ and obtain the dual optimal solution π_t^{kk}. This dual solution is added to a set Π of previously discovered optimal dual vectors (Step 6). Linear programming duality ensures that for an arbitrary scenario ω_t^j, a dual solution $\pi \in \Pi$ will satisfy: $\pi^\top[b_t(s_t, \omega_t^j) - C_t x_t] \leq h_t(s_t, x_t, \omega_t^j)$ for all x_t. Thus, in Step 7, we identify a dual vector in π_t^{kj} that provides the best lower bounding approximation at $\{h_t(s_t, x_t, \omega_t^j)\}$, for previous scenarios ω_t^j, where $j < k$:

$$\pi_t^{kj} \in \arg\max\{\pi^\top[b_t(s_t, \omega_t^k) - C_t x_t^k] \mid \pi \in \Pi\}. \tag{19}$$

Note that, this calculation is carried out only for previous observations, as π_t^{kk} will provide the best lower bound for $h_t(s_t, x_t, \omega_t^k)$. We use these dual vectors $\{\pi_t^{kj}\}_{j \leq k}$ to generate a lower bounding affine function for the k-th SAA. The coefficients of this affine function are given by:

$$\alpha_t^{kk} = \frac{1}{k}\sum_{j=1}^{k} (\pi_t^{kj})^\top [b_t(s_t, \omega_t^j)], \qquad \beta_t^{kk} = c_t - \frac{1}{k}\sum_{j=1}^{k} C_t^\top (\pi_t^{kj}). \tag{20}$$

Similar affine functions are also generated for incumbent solution $\bar{x}_t^k$ which we denote as $\bar{\alpha}_t^{kk}$ and $\bar{\beta}_t^{kk}$. The role of the incumbent solution will be discussed later in this section.

This affine function plays a similar role as the optimality cuts in the L-shaped method with one critical difference. In the L-shaped method, the optimality cut added in each iteration is guaranteed to be a supporting hyperplane to the expected recourse function. Therefore, the collection of all optimality cuts together provide a lower bounding function. In SD, on the other hand, with increasing iterations we use a larger number of scenarios to generate the approximation in (18). This implies that the affine piece computed at iteration $j < k$ lower bounds the sample mean $H_t^j(s_t, x_t)$, and not $H_t^k(s_t, x_t)$. As a result, the earlier affine pieces

need to be re-adjusted to ensure that they continue to provide lower bounds on the current sample mean $H_t^k(s_t, x_t)$. If we assume, without loss of generality, that $h_t(s_t, x_t, \tilde{\omega}_t) \geq 0$ (almost surely), then we have $H_t^k(s_t, x_t) \geq \frac{j}{k} H_t^j(s_t, x_t)$ for $j = 1, \cdots, k-1$. Hence, the previously generated affine functions are updated by multiplying them by a factor of $\frac{j}{k}$:

$$\alpha_t^{kj} = \frac{j}{k}\alpha_t^{jj} = \frac{k-1}{k}\alpha_t^{(k-1)j}, \qquad \beta_t^{kk} = \frac{j}{k}\beta_t^{jj} = \frac{k-1}{k}\beta_t^{(k-1)j}. \tag{21}$$

These updates are implemented using the recursive form as shown in (21). It follows that the approximation for the first-stage objective function at iteration k is given by:

$$f_t^k(s_t, x_t) := \max_{j=1,\cdots,k} [\alpha_t^{kj} + (\beta_t^{kj})^\top x_t] + \ell_t(s_{t+1}). \tag{22}$$

This approximation is used to obtain the next candidate solution by solving a regularized master problem in Step 10. The proximal term in the regularized problem uses an incumbent solution $\bar{x}_t^k$ which is the best solution discovered by the algorithm through iteration k. This is updated with the current solution ($\bar{x}_t^{k+1} = x_t^{k+1}$) if the (sample mean) point estimate of the objective value at x_t^{k+1} is better than the estimate at $\bar{x}_t^k$; else, $\bar{x}_t^{k+1} = \bar{x}_t^k$ (Higle and Sen (1994)).

Algorithm 1 Stochastic Decomposition

1: **Input** State variable s_t, dual multiplier set Π, scenario set Ω, iteration counter k.
2: **function** SD($s_t, \Pi \leftarrow \emptyset, \Omega \leftarrow \emptyset, k \leftarrow 0$)
3: **while** Stopping rule not met **do**
4: Update iteration counter $k \leftarrow k + 1$.
5: Simulate a new scenario ω_t^k independent of previously observed scenarios and collect it in $\Omega \leftarrow \Omega \cup \omega_t^k$.
6: Set up a subproblem $h_t(s_t, x_t, \omega_t^k)$, solve and collect the optimal dual vector π_t^{kk} in $\Pi \leftarrow \Pi \cup \pi_t^{kk}$.
7: Identify a dual vector π_t^{kj} that defines the best lower bound using (19).
8: Generate k-th lower bounding affine function using using (20) and update the previous affine functions using (21).
9: Update the first-stage objective function approximation to obtain $f_t^k(s_t, x_t)$ using (22).
10: Solve the master problem to obtain the next candidate solution x_t^{k+1} as:

$$x_t^{k+1} \leftarrow \text{argmax}\{f_t^k(s_t, x_t) + \frac{1}{2}||x_t - \bar{x}_t^k||^2 \mid x_t \in \mathcal{X}_t(s_t)\}.$$

11: Update incumbent solution $\bar{x}_t^k$.
12: **end while**
13: **return** $\bar{x}_t^{k+1}$, Π, Ω, $k+1$.
14: **end function**

Deterministic algorithms which solve convex programs by constructing an outer linearlization of the objective function (such as the L-shaped method) are terminated when the difference between the objective function value at a given iterate x_t^k and a valid lower bound on the objective function value is sufficiently small. The lower bounds obtained by SD are based on sampled information, and hence are stochastic. Therefore, deterministic termination criterion cannot directly be applied to a sampling-based algorithm. The SD approach uses a bootstrapping method to assess the primal-dual gap stability. The algorithm also gauges the impact of new information (new outcome ω_t^k, new first-stage candidate solution x_t^k, and new dual solution π_t^{kk}) on the approximation. A measure of this impact and the primal-dual gap stability are used in designing the stopping rules for SD. The SD algorithm obtains asymptotically accurate objective

function value estimates (with probability one) and generates a sequence of incumbent solutions which converge to an optimal solution (w.p.1). We refer the reader to (Higle and Sen, 1994) and (Sen and Liu, 2016) for detailed exposition on these stopping rules and convergence analysis.

The SD algorithm has several intrinsic traits which make it an attractive framework for the application considered in this work. We will end our description of this algorithm with the following two observations:

- SD theory (Higle and Sen (1994)) suggests that asymptotic convergence can be achieved by solving just one second-stage (15) in any iteration. In addition to that, efficient implementation of (19) and (20), and use of the appropriate data structure was recommended in (Higle and Sen, 1996) and Gangammanavar et al. (2019). These features allow SD to be used for large-scale stochastic optimization problems, often encountered in power systems operations, using minimal computational resources. This advantage was illustrated for a large-scale power system application in (Gangammanavar et al., 2016).

- Since SD works by introducing new scenarios in every iteration, it can easily be employed with external simulators. This allows updated forecast scenarios to be included without having to restart the optimization. For this reason, it is an ideal setting for our application where scenarios are generated by simulating a statistical model such as in §2.5.

3.2 Rolling-horizon SD Algorithm with Warm-starting Scheme

In our application, the coarse time period decisions are solutions to a 2-SLP given in §2.6. Over problem horizon $\mathcal{T}$, the 2-SLPs are solved multiple times in a rolling-horizon manner. The sequence of events at time period t is as follows: a) the SD algorithm is used to identify the optimal first-stage decision x_t^*, b) the recourse response y_t to this first-stage decision is computed along the true observation $\bar{\omega}_t$, and c) the state of the next period s_{t+1} is constructed to setup the next optimization problem. Since the SD algorithm allows for dynamic scenario selection, it conforms with the notion of adaptation over time. This allows us to design effective warm-starting procedures. We use information from the optimization model in a previous time period to create an initial approximation. We refer to this pre-optimization procedure as warm-starting.

Recall that the stochastic process considered in our application follows the linear model presented in §2.5. During optimization, the SD algorithm uses simulation to generate one new scenario at each iteration as described in Step 5. This simulation is carried out by generating the noise process $\{\epsilon_\tau\}$ and computing the scenario using (2.5). During the algorithm, the simulated noise observations are collected in the set Ξ along with the set of dual solutions Π. We make the following observations:

- The subproblem in (15) has fixed recourse, as the randomness affects only the right-hand side of constraints, and the recourse matrix D is time-invariant. This implies that the subproblem's dual feasible region is not affected by randomness and is fixed for all $t \in \mathcal{T}$. Hence, a dual solution $\pi \in \Pi$, obtained during the SD solve for time period t is feasible for other time periods.

- Recall that the stochastic processes in §2.5 can be decomposed into deterministic and stochastic components as in (13). Further, the noise process $\tilde{\epsilon}_\tau$ used in the ARMA model is distributionally time-invariant. Therefore, the noise ϵ_τ simulated during the SD solve to generate scenario ω_t^k for time period t can be used to generate scenarios using (12) for future time periods.

The SD algorithm uses regularizing terms in the master problem objective function (see Step 10 of Algorithm 1). This allows us to specify a finite number of cuts (number of first-stage decisions + 3) to be retained without sacrificing the optimality of the limiting incumbent solution. We refer the reader to (Higle and Sen, 1994) for more details regarding the finiteness

of the SD master problem. This also implies that only a subset of cuts are active at optimality (say for time period $t-1$). We use this subset of cuts to build an initial approximation for time period t. We denote this subset as $\mathcal{J}_t$. Recall that SD cuts are based on a certain set of scenarios where each scenario is associated with a noise term $\epsilon_t^j \in \Xi$.

For cut $m \in \mathcal{J}_t$, let $E^m \subseteq \Xi$ denote the noise observation used to generated the cut. We use this set, along with the true observation $\bar{\omega}_{t-1}$, to re-generate scenarios using (13). The scenarios are stored in their decomposed form ($\bar{\Gamma}_t$ and $\Delta\tilde{\Gamma}_t$) which in turn are used to build the right-hand side given in (16). With these, the coefficients of warm-start cut m are computed as:

$$\alpha_t^m = \frac{|E^m|}{|\Xi|} \sum_{j=1}^{|E^m|} (\pi_t^{mj})^\top [\bar{b}_t(s_t, \bar{\Gamma}_t) + \Delta b_t(\Delta\Gamma_t^j)], \tag{23a}$$

$$\beta_t^m = c_t - \frac{|E^m|}{|\Xi|} \sum_{j=1}^{|E^m|} C_t^\top (\pi_t^{mj}). \tag{23b}$$

The set of warm-start cuts define the initial piecewise linear approximation:

$$f_t^0(s_t, x_t) = \max_{m=1,\dots M} \{\alpha_t^m + (\beta_t^m)^\top x_t\} + \ell_t(s_{t+1}). \tag{24}$$

The warm-start approximation is computed for $t > 0$ and for the first coarse time period we use $f_0^0(s_0, x_0) = 0$. The multiplier $\frac{|E^m|}{|\Xi|}$ in (23) serves the same purpose as the $\frac{j}{k}$ factor in (21). The warm-started cut m is based on $|E^m|$ noise observations, whereas we have $|\Xi|$ total noise observations. The cuts in $\mathcal{J}$ are based on different numbers of noise observations, and the multiplier ensures that all of these cuts provide a valid lower bound to our problem at time period t.

Note that the calculations involving $\bar{b}_t$ and $\epsilon_t^j \in E^m$ in (23) are simplified using information from the previous time period. Therefore, new calculations are carried out only with respect to the state s_t. Efficient utilization of past information depends on the appropriate design and implementation of a data structure. To accomplish this, we extend the SD data structure in (Higle and Sen, 1996). This reduces the computational requirement for our warm-starting scheme[3].

The warm-starting scheme used in time period t is outlined in Algorithm 2, and the overall stochastic computational framework is presented in Figure 4. To summarize, given a state s_t at time period $t \in \mathcal{T}$, we begin by obtaining an initial approximation using the warm-starting procedure in Algorithm 2. The SD algorithm uses this initial lower bounding approximation $f_t^0(s_t, x_t)$ in Step 11, updates this approximation by incorporating additional samples (if necessary), and obtains the optimal solutions x_t^*. The additional samples (ω_t, blue curves) are generated by simulating the noise process $\tilde{\epsilon}_t$ and using the historical/true observation ($\bar{\omega}_{t-1}$, red curve) in Figure. 4. The decision x_t^* is implemented, the recourse decision $y_t(\bar{\omega}_t)$ is computed by solving the subproblem (15) with input $(s_t, x_t^*, \bar{\omega}_t)$, and thereby setting the state for the next time period $s_t = [x_t^*, y_t(\bar{\omega}_t)]$. This process is repeated until the end of the horizon.

Remark: The convergence of outer-linearization algorithms, such as Benders decomposition, depends on the discovery of "relevant" dual solutions from a finite set of extreme points. A warm-starting procedure, similar to the one described in Algorithm 2, can be used with the L-shaped algorithm as well. As t increases, the number of dual solutions discovered will also increase, as will the quality of initial approximation. This reduces the burden of re-discovering the dual solution in every time period.

Remark: The renewable generation and demand scenarios simulated using the statistical model described in §2.5 may result in negative values. In order to satisfy the zero lower bound

[3]For brevity, we do not present our implementation details in the paper and refer the reader to our source code available at `https://github.com/jac0320/rollingSD`.

Algorithm 2 SD algorithm with warm-starting scheme

Input: State variable s_t, previous optimal first-stage decision x^*_{t-1}, dual vector set Π, sampled noise set Ξ, warm-starting cut set $\mathcal{J}_t$.
function WarmStartingSD($s_t, x^*_{t-1}, \Pi, \Xi, \mathcal{J}_t$)
  for $m \in \mathcal{J}_t$ **do**
    Collect noise observations subset $E^m \subseteq \Xi$.
    for $\epsilon^j \in E^m$ **do**
      Re-construct scenario ω_t^j using (13)
      Identify and collect the best dual vector for each re-constructed scenario

$$\pi_t^{mj} \in \text{argmax}\{\pi^\top [b_t(s_t, \omega_t^j) - C_t x^*_{t-1}] \mid \pi \in \Pi\}.$$

    end for
    Warm-start lower bounding cut m using (23).
  end for
  Construct the warm-start initial piecewise linear approximation $f_t^0(s_t, x_t)$ using (24).
  return f_t^0
end function

requirement of these quantities, we introduce an auxiliary parameter κ_t to truncate the negative value (see Appendix A for details). This truncation has to be accommodated during the warm-start procedure. This is achieved by incorporating an additional term with κ_t in the coefficient computation α_t^m step in (23):

$$\alpha_t^m = \frac{|E^m|}{|\Xi|} \sum_{j=1}^{|E^m|} (\pi_t^{mj})^\top [\bar{b}_t(s_t, \bar{\Gamma}_t) + \Delta b_t(\Delta \Gamma_t^j) + \kappa_t^j]. \tag{25}$$

A similar procedure is adopted for truncating simulated scenarios when values exceeds the rated power (e.g., the cut-out speed for wind generation).

4 Computational Experiments

In this section, we present the computational experiments conducted on our MS-RR framework. We will first describe the experimental setup used, and then, discuss the results from these experiments. The experiments are designed to answer the following questions:

- What are the advantages of our stochastic framework in comparison to a deterministic approach, which uses a single forecast?
- What are the computational advantages of the SD algorithm over the traditional SAA method with a fixed number of scenarios, and how is it beneficial for our application?
- What advantages does the warm-starting scheme provide to enable stochastic programming algorithms to be applied for power systems applications?
- In §1, we listed a few deterministic and probabilistic rules for determining reserve requirements. Is it possible to identify a simple rule that provides the best results over the entire horizon? Moreover, how do the MS-RR solutions and objective function values compare to those obtained from the fixed rules?

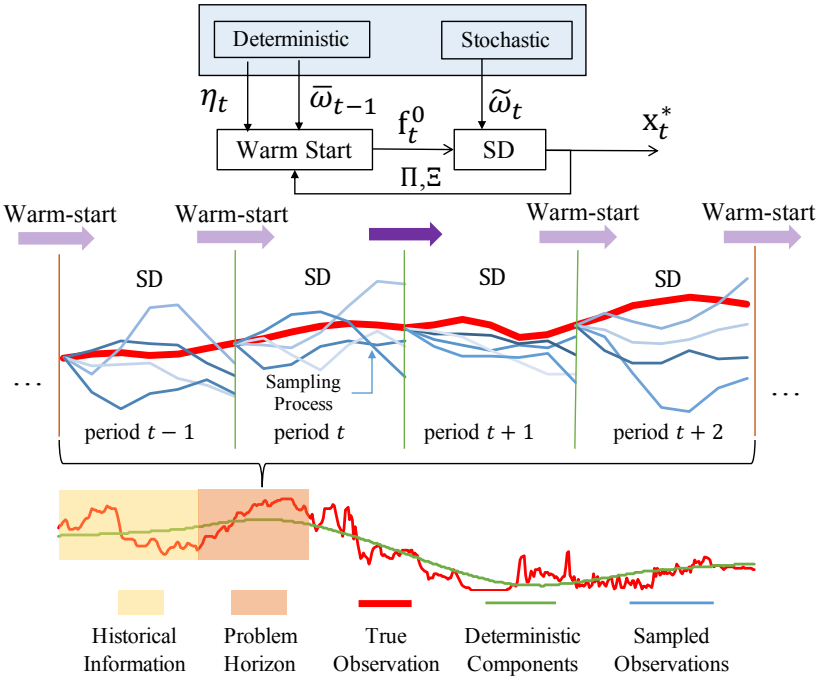

Figure 4: Graphical Representation of Algorithm 1

4.1 Experimental Setup

Although the operating practices differ significantly across ISOs/BAAs, the principal components include DA-UC, ST-UC and hour-ahead ED as in (Makarov et al., 2010). The operating reserves are usually committed during the ST-UC stage, which involves solving MIPs every 4 to 6 hours. Our primary goal is to establish requirements (position the generation levels) of these committed reserves, and hence we consider a six-hour horizon in our instances. The commitments are fixed over this horizon and are considered as inputs to the model. For all the instances, the look-ahead horizon was set to six hours at two-hour resolutions, and a single forecast scenario was used for net-demand in the look-ahead horizon.

Test Systems

Two modified test energy networks, IEEE 118 and IEEE 300, are used in this study. These test instances and stochastic process models are also available on the Github repository. These networks are modified by incorporating wind farms for renewable energy generation. The IEEE 118 has 118 buses, 186 transmission lines, and 39 generation units, of which 18 units are assumed to provide regulating services. Three wind farms are incorporated as renewable resources, which account for 26% penetration. As for the larger IEEE 300, there are 300 buses, 411 transmission lines, and 69 generation units, where 38 generators act as regulating reserves. Five wind farms are included in this network with the penetration level set to 27%.

Stochastic Processes

Our proposed formulation §2 allows both renewable energy generation and demand to be stochastic and are described by the general form in §2.5. The wind generation model was built using data from WWSIS (Potter et al. (2008)). The original dataset comprises wind speed and power data for 2006 at 10-minute resolution. This data was preprocessed by (a) decomposing it into trend, seasonality and residual process, and (b) verifying stationarity of residual processes. Therefore, this preprocessed data was used to estimate parameters for our multivariate ARMA model.

We used time series libraries (`stl` by (Cleveland et al., 1990), `MTS` by (Tsay, 2005), `KPSS` by (Kwiatkowski et al., 1992), etc.) in the statistical package R to accomplish these tasks. Based on our analyses ARMA$(2,0)$ and ARMA$(3,0)$ models were found to be adequate to represent wind generation in IEEE 118 and IEEE 300 test systems respectively[3]. Since the variability in demand is significantly lower than renewable energy generation, we ignore demand uncertainty in the instances studied here. To accommodate demand variation over time, the original demand data is modified according to trend pattern for a winter weekday based on data available in (Grigg et al., 1999).

Platform

Our algorithm is developed in C and we use the IBM ILOG CPLEX 12.6.1 callable library to optimize all linear and quadratic programs encountered during the solution process. The experiments are conducted on a 64-bit Intel-Core i5 CPU @2.50GHz with 16 GB of RAM.

Solution Verification Process

The outcomes of our model are a first-stage solution incorporating operation schedules of large-capacity generation and reserve requirements with an estimated cost. To verify the quality of a solution, we employ posterior examination by fixing the first-stage decisions and simulating the second-stage recourse function. The first-stage decisions are obtained from a LP solve when deterministic settings or SAA is used, and from the SD algorithm when a stochastic setting is applied. The scenarios used for verification are generated independent of the scenarios used for optimization. This procedure is sometime referred to as "out-of-sample verfication". The verification is carried out until the variance of the expected recourse value is within an acceptable limit. We report the optimal objective function value obtained from the optimization step as the predicted value, mean, and an $\alpha = 0.05$ confidence interval (CI) obtained from verification step in our results presentation. When the predicted value obtained from optimization is close to the verification CI, the solution to a SP model is deemed as acceptable.

4.2 Comparison of Computational Frameworks

At the onset, we will establish the value of our MS-RR framework compared to its deterministic counterpart. In order to do this, we set up the deterministic RR (D-RR) framework by replacing the random variable in our formulation in §2 by the single forecast. This results in a deterministic linear program at each time period that can be solved using off-the-shelf solvers.

We compare the solution obtained from D-RR and MS-RR frameworks by evaluating them over the same set of scenarios. These results are summarized in TABLE 1 for IEEE 118. The predicted value is the optimal objective function value reported by the solver, and the verification results include the mean and the 95% CI. The last column indicates the optimistic error (relative gap between CI deviation of predicted value and evaluated mean). Due to the inherent stochasticity, it is not guaranteed that the predicted value always falls within the verification CI. But when it does, then the cost associated with that solution is more reliable. As can be seen, the results from the D-RR are more likely to be erroneous when compared to MS-RR results. The actual observation can be significantly different from the forecast used in deterministic framework, which is historically the case when renewable resources are incorporated. The use of only one forecast leads to a biased representation of the future, and therefore, the predicted value is not the same as the verification result. Our SD based framework overcomes this by sampling observations until sufficient confidence is built on the predicted value.

	t	Predicted Value ($)	Number of Scenarios	Verification		
				CI Mean(k$)	95% CI (k$)	Err.%
MS-RR	1	222,779.4	305	227.4	[226.3, 228.6]	1.53
	2	230,699.2	282	230.2	[229.1, 231.4]	-
	3	316,182.6	258	315.0	[313.4, 316.7]	-
	4	269,101.7	266	274.3	[273.0, 275.7]	1.43
	5	264,297.9	265	258.5	[257.2, 259.8]	1.73
	6	260,087.6	280	259.4	[258.1, 260.8]	-
D-RR	1	189,729.6	1	241.2	[238.8, 243.7]	20.33
	2	251,289.4	1	235.2	[232.9, 237.5]	5.88
	3	405,777.3	1	324.7	[321.3, 328.1]	23.91
	4	322,422.4	1	299.2	[296.1, 302.9]	6.73
	5	310,839.2	1	293.6	[290.2, 296.7]	4.82
	6	219,816.9	1	289.4	[286.2, 292.6]	22.93

Table 1: MS-RR and D-RR Comparison

4.3 Comparison of Algorithmic Approaches

Based on our discussion in the previous experiment, the advantage of our stochastic framework is undeniable. In this experiment, we compare our SD approach to SAA-based conventional SP approach. When compared to fixed scenario SAA, the critical advantage of the SD algorithm is the dynamic stopping criteria which allows for on-the-fly determination of the number of scenarios. In order to illustrate this advantage, we conducted experiments for our application which compare results from SAA with varying scenario size to those from the SD algorithm in Figure 5.

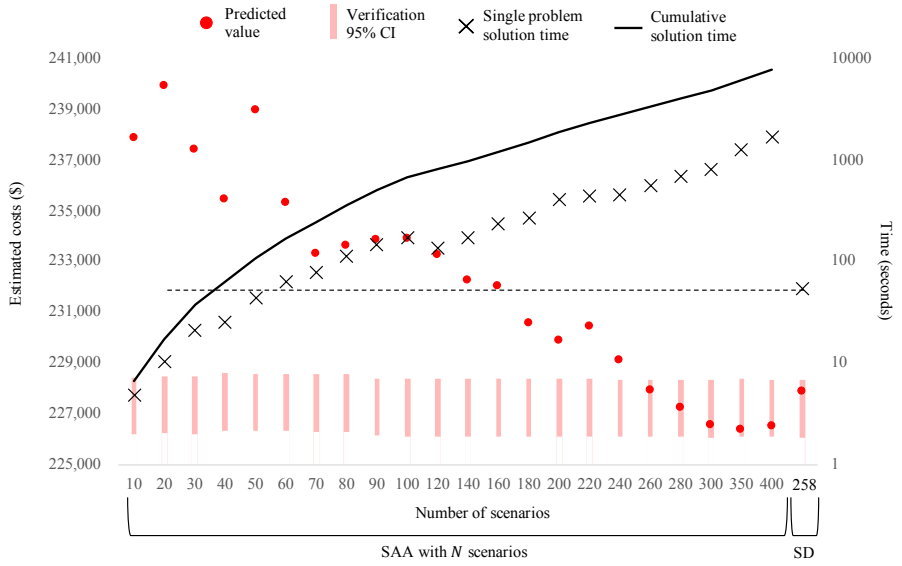

Figure 5: Comparison of SAA with varying scenario size and SD algorithm using IEEE 118 system

Notice that the predicted values from SAA with small scenario size ($S < 200$) are significantly different from the verification CI, and therefore the quality of these solutions are suspect. On the other hand, when sample size increases, the gap between the predicted and verification values decreases. In fact for $S > 260$, the SAA procedure results in solutions whose predicted value falls within the verification CI. However, the Figure 5 also shows that computation time increases

with scenario size. The SD algorithm, on the contrary, identifies an acceptable solution with significantly lower computational time (~ 53 seconds, compared to ~ 552 seconds for SAA with $S = 260$ samples).

The ideal scenario size for SAA is not known until sequential experiments are conducted with increasing scenario size. Figure 5 shows the cumulative time of performing these sequential experiments. Note that the experiment requires > 3000 CPU seconds before identifying an acceptable solution. We recognize that cumulative time depends on the sequence of scenarios size S selected for experiment. Nevertheless, one cannot overcome the need for this sequential procedure to identify the ideal scenario size. Moreover, even for a given scenario size which results in acceptable solutions, the SD algorithm outperforms SAA computationally (e.g., $S = 260$).

4.4 Advantage of Warm-Starting

	Total Number of Scenarios		Running Time(s)		WS Time(s)	Dual Re-used	LP Solved		Simulated Noise	
t	WS	NWS	WS	NWS	WS	WS	WS	NWS	WS	NWS
IEEE 118										
1	305	305	106	106	0.00	0	305	305	1830	1830
2	504	282	63	95	0.09	8	199	282	1194	1692
3	685	258	53	77	0.14	23	181	258	1086	1548
4	866	266	57	85	0.20	58	181	266	1086	1596
5	1029	265	47	79	0.27	74	163	265	978	1590
6	1210	280	57	98	0.34	45	181	280	1086	1680
IEEE 300										
1	277	277	312	312	0.00	0	277	277	1662	1662
2	677	476	659	843	0.15	0	400	476	2400	2856
3	988	361	410	495	0.35	156	311	361	1866	2166
4	1327	424	488	665	0.46	310	339	424	2034	2544
5	1612	392	357	601	0.58	208	285	392	1710	2352
6	1950	375	479	510	0.80	114	338	375	2028	2250

Table 2: Warm-starting Scheme Comparison Summary

Practical implementation of RR must adhere to the strict time requirements set by the ISOs/BAAs (which range from $5-15$ minutes). Such requirements pose significant challenges for stochastic approaches due to the computational intractability. This overshadows the benefits of using these approaches. In §3, we proposed a warm-starting mechanism to address this concern. To illustrate its advantage, we solve a more extensive test case, IEEE 300, in this experiment. The results are summarized in TABLE 2. In the table, WS denotes warm-starting while NWS means the opposite. Recall that our warm-starting scheme depends on efficiently re-utilizing observations and dual information. Therefore, the number of scenarios for WS cumulatively increases, and a significant number of dual solutions are re-utilized. Warm-starting avoids the need for re-discovering the duals. Hence, the number of LPs solved is reduced as indicated in the table. As a consequence, computation time is reduced by 36% on average for IEEE 118 and the total number of LPs solved is 27% less. For the larger IEEE 300 test network, computation time and the number of LPs solved decreased by 22% and 15%, respectively.

4.5 Regulating Reserves Requirement Study

In practice, reserve requirements are established using certain fixed rules to satisfy system reliability concerns. These rules vary across ISOs balancing areas. In this experiment, we compare our MS-RR framework with three such rules:

4.5.1 Rule 1: Largest Renewable Capacity

This conservative rule considers the possibility of losing all online renewable infeed. It prepares the system by including spinning reserves whose capacity is at most the available spinning reserve capacity or the nameplate renewable energy generation capacity.

4.5.2 Rule 2: Deviation of the Net-Demand

This rule requires a certain multiple of the forecast net-demand standard deviation to be available at all times. Similar rules are being practiced in NYISO and PJM regions (Erik et al. (Aug. 2011)). In our experiments, we consider 3.5 times the standard deviation of the net-demand to be required as in (Ortega-Vazquez and Kirschen, 2009).

4.5.3 Rule 3: Proportional Reserves Capacity

This rule mandates a certain portion of the spinning reserves to be online for correcting system imbalances. The portion is established ahead of time and is fixed over the entire horizon. We experiment with different portions (5%, 10%, 20%, 40%) to explore how this choice effects the objective estimate, and compare them with our stochastic framework. Such options are currently in practice in the ERCOT region (Erik et al. (Aug. 2011)). All the three rules were tested using

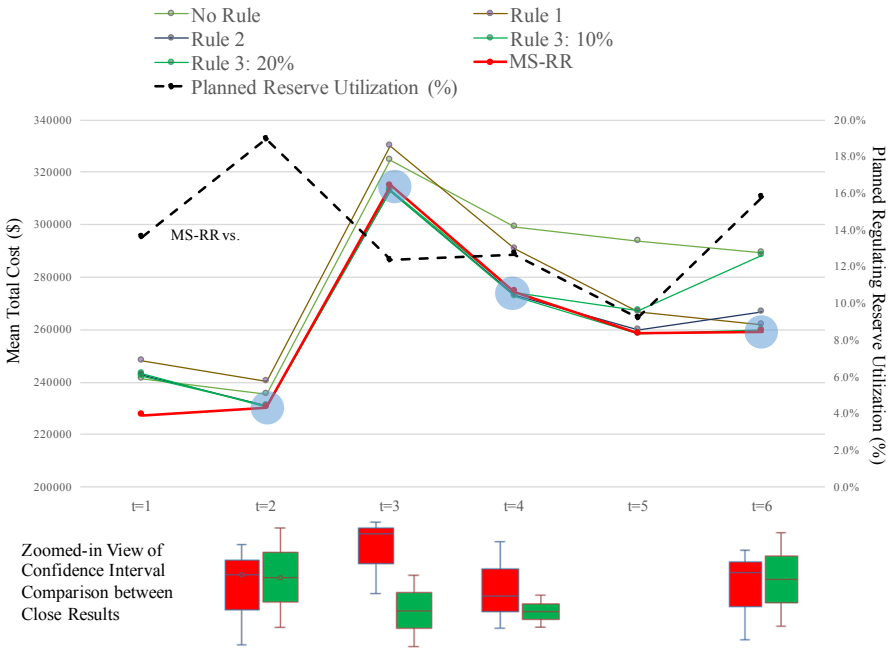

Figure 6: Objective Comparison with Deterministic Rules

D-RR framework with IEEE 118 test network. The solutions were evaluated as before, and the results are presented in TABLE 3 and Figure. 6. In the figure, the mean verification values are plotted using the solid red line for each approach over the entire horizon. The figure also shows verification CIs for MS-RR and D-RR when a rule-based approach yields a lower mean

verification value when compared to MS-RR. We extract the best rule-based approach, and present its verification results in TABLE. 3.

Our MS-RR framework provides cost-efficient reserve requirement recommendations by considering an appropriate number of scenarios while maintaining system reliability. Since the level of uncertainty varies over time, the need for reserves also fluctuates. The MS-RR framework identifies this variation in requirements, and therefore, provides recommendations that vary over time (indicated by the dotted line in Figure. 6). The rule-based approaches for D-RR lack such a flexibility. This is reflected in high costs associated with Rules 1 and 2. As for Rule 3, its success depends on choosing the appropriate portion ahead of time. For the IEEE 118 instance tested, the verification value when the portion was set to 20% was statistically comparable to the MS-RR results. In fact, it yielded better (by 2%) value than MS-RR for time period 3. However, there is no guarantee that 20% will be appropriated for other time periods, in other test systems, or when the underlying stochastic process changes (e.g., due to weather). This was indeed the case for time periods 1 and 6, when other rules turn out to be better.

t	Best Fixed Rule for D-RR Framework			Outperforms MS-RR?
	Rule	CI Mean ($)	95% CI ($)	
1	NO Rule	241,242.7	[238,771.6, 243,713.8]	No
2	Rule 3: 20%	230,639.8	[229,534.9, 231,744.7]	No
3	Rule 3: 20%	312,660.9	[311,029.1, 314,292.7]	Yes
4	Rule 3: 20%	272,754.1	[271,399.4, 274,108.9]	No
5	Rule 3: 20%	258,557.8	[257,235.4, 259,880.4]	No
6	Rule 3: 40%	259,662.8	[258,273.7, 260,151.8]	No

Table 3: Comparison of Best Deterministic Rules to MS-RR

5 Conclusions and Future Research

In this paper, we presented a novel MS-RR framework that will assist system operators for economically dispatching different energy resources, including planned operating reserves. While such a framework is suitable for a wide range of dispatch operations (including ED), we used it to obtain statistical estimates of various reserve requirements. Our framework provides recommendations for planning: following, regulating and ramping reserves in a system with significant renewable penetration while honoring physical operating constraints of generators and the power network. We tackle this multi-period problem using a scalable rolling horizon approach with dynamic states and look-ahead approximations. Our computational results showed the deficiency of D-RR framework when optimizing systems that are exposed to significant variability and uncertainty. Our stochastic approach was successful in reducing the bias and thereby resulted in solutions that are statistically better. Our experiments with different rule-based methods illustrated that no single rule consistently yielded good results over all time periods and instances. Our MS-RR approach, on the other hand, provided the necessary flexibility to determine the requirements in a dynamic and cost efficient manner while ensuring system reliability. Finally, to achieve the time requirements in real-world, we proposed warm-starting extensions for the SD algorithm and showed this mechanism to be effective on large networks with high renewable penetration.

In the future, we will verify the performance of our approach on real-scale power networks by extending our framework to include AC power flows. We will also investigate the role of storage devices in reducing the reserve requirements. Currently, the framework horizon is restricted to be between commitment changes. Integrating the commitment decisions mandates that techniques that allow commitment decisions to change within the MS-RR framework be in-place.

Introduction of commitment decisions and coupling these decisions across commitment horizons (e.g. 24-hour for DA-UC) introduces binary decision variables that pose great algorithmic challenges. We are currently exploring these enhancements to our MS-RR framework, and results from this study will be reported in our future work. The operating reserve estimation problem is truly a multistage stochastic optimization problem, particularly when the goal is to estimate the multiperiod ramping capability. We will explore the possibility of applying the stochastic dynamic linear programming algorithm (Gangammanavar and Sen, 2019), a multistage extension of the two-stage SD algorithm to tackle the multistage problem.

References

Ahmadi-Khatir A, Conejo AJ, Cherkaoui R (2014) Multi-area unit scheduling and reserve allocation under wind power uncertainty. IEEE Trans on Power Systems 29(4):1701–1710

Atakan S, Gangammanavar H, Sen S (2019) Operations planning experiments for power systems with high renewable resources. Tech. rep., Southern Methodist University

Birge JR, Louveaux F (2011) Introduction to Stochastic Programming. Springer Series in Operations Research and Financial Engineering, Springer

Bouffard F, Galiana FD (2004) An electricity market with a probabilistic spinning reserve criterion. IEEE Trans on Power Systems 19(1):300–307

Brown BG, Katz RW, Murphy AH (1984) Time series models to simulate and forecast wind speed and wind power. Journal of Climate and Applied Meteorology 23(8):1184–1195

Chattopadhyay D, Baldick R (2002) Unit commitment with probabilistic reserve. In: Power Engineering Society Winter Meeting, 2002. IEEE, IEEE, vol 1, pp 280–285

Cleveland RB, Cleveland WS, Terpenning I (1990) Stl: A seasonal-trend decomposition procedure based on loess. Journal of Official Statistics 6(1):3

Dantzig GB, Wolfe P (1960) Decomposition principle for linear programs. Operations Research 8(1):101–111, DOI 10.1287/opre.8.1.101, URL `http://dx.doi.org/10.1287/opre.8.1.101`, `http://dx.doi.org/10.1287/opre.8.1.101`

Dvorkin Y, Pandžić H, Ortega-Vazquez MA, Kirschen DS (2015) A hybrid stochastic/interval approach to transmission-constrained unit commitment. IEEE Trans on Power Systems 30(2):621–631

Erik E, Milligan M, Kirby B (Aug. 2011) Operating reserves and variable generation. NREL Technical Report

Gangammanavar H, Sen S (2019) Stochastic dynamic linear programming: A sampling based algorithm for multistage programs. Tech. rep., Southern Methodist University

Gangammanavar H, Sen S, Zavala VM (2016) Stochastic optimization of sub-hourly economic dispatch with wind energy. IEEE Transactions on Power Systems 31(2):949–959

Gangammanavar H, Liu Y, Sen S (2019) Stochastic decomposition for two-stage stochastic linear programs with random cost coefficients. IINFORMS Journal on Computing (accepted) To appear in INFORMS Journal on Computing

Grigg C, Wong P, Albrecht P, Allan R, Bhavaraju M, Billinton R, Chen Q, Fong C, Haddad S, Kuruganty S, Li W, Mukerji R, Patton D, Rau N, Reppen D, Schneider A, Shahidehpour M, Singh C (1999) The IEEE reliability test system-1996. a report prepared by the reliability test

system task force of the application of probability methods subcommittee. IEEE Transactions on Power Systems 14(3):1010–1020, DOI 10.1109/59.780914

Hamilton JD (1994) Time series analysis, vol 2. Princeton university press, Princeton, NJ

Higle JL, Sen S (1994) Finite master programs in regularized stochastic decomposition. Mathematical Programming 67(1-3):143–168

Higle JL, Sen S (1996) Stochastic Decomposition: A Statistical Method for Large Scale Stochastic Linear Programming. Kluwer Academic Publishers, Boston, MA.

Kwiatkowski D, Phillips PC, Schmidt P, Shin Y (1992) Testing the null hypothesis of stationarity against the alternative of a unit root: How sure are we that economic time series have a unit root? Journal of Econometrics 54(1-3):159–178

Linderoth J, Shapiro A, Wright S (2006) The empirical behavior of sampling methods for stochastic programming. Annals of Operations Research 142(1):215–241, DOI 10.1007/s10479-006-6169-8, URL http://dx.doi.org/10.1007/s10479-006-6169-8

Makarov Y, Guttromson R, Huang Z, Subbarao K, Etingov P, Chakrabarti B, Ma J (2010) Incorporating wind generation and load forecast uncertainties into power grid operations. Report PNNL-19189, PNNL

Morales J, Minguez R, Conejo A (2010) A methodology to generate statistically dependent wind speed scenarios. Applied Energy 87(3):843 – 855, DOI 10.1016/j.apenergy.2009.09.022

Motto AL, Galiana FD, Conejo AJ, Arroyo JM (2002) Network-constrained multiperiod auction for a pool-based electricity market. IEEE Trans on Power Systems 17(3):646–653

Olson A, Mahone A, Hart E, Hargreaves J, Jones R, Schlag N, Kwok G, Ryan N, Orans R, Frowd R (2015) Halfway there: Can california achieve a 50% renewable grid? IEEE Power and Energy Magazine 13(4):41–52

Ortega-Vazquez MA, Kirschen DS (2009) Estimating the spinning reserve requirements in systems with significant wind power generation penetration. IEEE Transactions on Power Systems 24(1):114–124, DOI 10.1109/TPWRS.2008.2004745

Papavasiliou A, Oren S (2013) Multiarea stochastic unit commitment for high wind penetration in a transmission constrained network. Operations Research 61(3):578–592, DOI 10.1287/opre.2013.1174, URL http://dx.doi.org/10.1287/opre.2013.1174, http://dx.doi.org/10.1287/opre.2013.1174

Papavasiliou A, Oren S, O'Neill R (2011) Reserve requirements for wind power integration: A scenario-based stochastic programming framework. IEEE Transactions on Power Systems 26(4):2197–2206

Potter CW, Lew D, McCaa J, Cheng S, Eichelberger S, Grimit E (2008) Creating the dataset for the western wind and solar integration study (U.S.A.). Wind Engineering 32(4):325–338, http://wie.sagepub.com/content/32/4/325.full.pdf+html

Powers JG, Klemp JB, Skamarock WC, Davis CA, Dudhia J, Gill DO, Coen JL, Gochis DJ, Ahmadov R, Peckham SE, Grell GA, Michalakes J, Trahan S, Benjamin SG, Alexander CR, Dimego GJ, Wang W, Schwartz CS, Romine GS, Liu Z, Snyder C, Chen F, Barlage MJ, Yu W, Duda MG (2017) The weather research and forecasting model: Overview, system efforts, and future directions. Bulletin of the American Meteorological Society 98(8):1717–1737, DOI 10.1175/BAMS-D-15-00308.1, URL https://doi.org/10.1175/BAMS-D-15-00308.1, https://doi.org/10.1175/BAMS-D-15-00308.1

Price JE (2015) Evaluation of stochastic unit commitment for renewable integration in california's energy markets. In: Power & Energy Society General Meeting, 2015 IEEE, IEEE, pp 1–5

Rockafellar RT, Wets RJB (1991) Scenarios and policy aggregation in optimization under uncertainty. Math Oper Res 16(1):119–147

Sen S, Liu Y (2016) Mitigating uncertainty via compromise decisions in two-stage stochastic linear programming: Variance reduction. Operations Research 64(6):1422–1437

Sen S, Yu L, Genc T (2006) A stochastic programming approach to power portfolio optimization. Operations Research 54(1):55–72, http://dx.doi.org/10.1287/opre.1050.0264

Shapiro A, Dentcheva D, Ruszczynski A (2014) Lectures on Stochastic Programming: Modeling and Theory, Second Edition. Society for Industrial and Applied Mathematics, Philadelphia, PA, USA

Tsai H, Chan KS (2007) A note on non-negative arma processes. Journal of Time Series Analysis 28(3):350–360

Tsay R (2005) Analysis of financial time series, 2nd edn. Wiley series in probability and statistics, Wiley-Interscience, Hoboken, NJ, URL http://gso.gbv.de/DB=2.1/CMD?ACT=SRCHA&SRT=YOP&IKT=1016&TRM=ppn+483463442&sourceid=fbw_bibsonomy

Van Slyke RM, Wets RJB (1969) L-shaped linear programs with applications to optimal control and stochastic programming. SIAM Journal on Applied Mathematics 17(4):638–663

Zavala VM (2016) New architectures for hierarchical predictive control. IFAC-Papers Online 49(7):43–48

Zheng QP, Wang J, Liu AL (2015) Stochastic optimization for unit commitment—a review. IEEE Transactions on Power Systems 30(4):1913–1924, DOI 10.1109/TPWRS.2014.2355204

A Statistical Model of Uncertainty

Wind power at any wind farm location can be described as a stochastic process. This process exhibits spatial correlation with processes describing wind power at other geographically separated wind farm locations. These processes are also temporally correlated across several time periods. Hence an appropriate description of these stochastic processes requires recognizing the spatio-temporal correlations of these processes.

The available wind power data is pre-processed by identifying the trend and seasonality. The seasonal-trend decomposition procedure based on Loses (STL, Cleveland et al. (1990)) is an appropriate method to achieve this. Once trend and seasonality is estimated, they are subtracted from the original time-series to obtain the residual time-series. Before proceeding, it is necessary to verify if this residual series is stationary. The Augmented Dick-Fuller test and KPSS test were used for this purpose (Hamilton (1994)). One possible choice to model a stationary time-series is the multivariate ARMA process shown in (12). A multivariate ARMA models was fitted using the MTS package (Tsay (2005)) in R. The order selection is based on Bayesian Information Criterion (BIC) as it is most suitable for data with limited length. The validity of the model is verified by checking the cross-covariance and correlation functions, and the whiteness of the residual process is verified using the Ljung-Box test.

Recall that our optimization framework relies upon a constant stream of simulated scenarios. The fitted ARMA model is used for this purpose. The simulation is carried out at fine timescale within the decision epoch $t \in \mathcal{T}$. Recall that we introduce time index τ in §2.5 to unify different time scales. At corresponding time index τ at time period $t \in \mathcal{T}$, we used historical data from

time period $(\tau - 1)$ as known information for this simulation (the red time series in Figure. 4). Once a residual time series is simulated, the estimated trend and seasonality is added back to obtain the wind power time series (the blue time series in Figure. 4). It should be noted that it is possible to obtain negative wind power values (particularly when trend values are small) using the above procedure. In order to address this, we truncate the simulated time series at zero: $\widetilde{W}_\tau = \eta_\tau + \tilde{\omega}_\tau + \kappa_\tau$, where $\kappa_\tau > 0$ when the simulated output is negative. It is necessary to emphasize the difficulty in constructing stationary processes with non-negative outcomes. There exists limited theoretical results in (Tsai and Chan, 2007) to address this. However, we enforce non-negativity as part of our algorithm in order to ensure model and algorithm validity.

While our presentation in this paper revolves around stationary residual processes, non-stationary processes can also be accommodated within our framework. In this sense, the proposed method is applicable in conjunction with any external simulator (e.g., the Weather Research and Forecasting Model Powers et al. (2017)).

B Notations

We will use $t \in \mathcal{T}$ to index the decision epochs and $n \in \mathcal{N}$ to index the fine time periods within decision epoch t.

Sets:

$\mathcal{B}$	buses
$\mathcal{L}$	transmission lines
$\mathcal{D}$	demand nodes
$\mathcal{W}$	renewable generators
$\mathcal{G}^B$	base-load generators
$\mathcal{G}^F/\mathcal{G}^S/\mathcal{G}^R$	following/regulating/ramping reserves

Stochastic Processes:

$\hat{L}_{tni}/\widetilde{L}_{tni}$	forecast/actual demand (MW) at $i \in \mathcal{D}$
$\widehat{W}_{tni}/\widetilde{W}_{tni}$	forecast/actual renewable generation (MW) at $i \in \mathcal{W}$
$\tilde{\omega}_t$	consolidated random vector
η_t	trend time series.

Parameters:

V_i	voltage (kV) of bus $i \in \mathcal{B}$
X_{ij}	reactance of transmission line $(i,j) \in \mathcal{L}$
c_i^b	unit generation (MW) cost of $i \in \mathcal{G}^B$
c_i^f	unit generation (MW) cost of $i \in \mathcal{G}^F$
c_i^s	unit generation (MW) cost of up-front dispatch $i \in \mathcal{G}^S$
c_i^p	unit cost of planning regulating service (MW) on $i \in \mathcal{G}^S$
d_i^s	unit cost of utilizing (MW) $i \in \mathcal{G}^S$
d_i^r	unit cost of utilizing (MW) $i \in \mathcal{G}^R$
$\Delta\hat{L}^{tni}$	net-demand (MW) base on available forecast of $i \in \mathcal{D}$
p^{min}, p^{max}	transmission line limitations (MW)
$\theta^{min}, \theta^{max}$	voltage angle limitations
$G_i^{b,min}$,$G_i^{b,max}$	min and max capacity (MW) of $i \in \mathcal{G}^B$
$G_i^{f,min}$,$G_i^{f,max}$	min and max capacity (MW) of $i \in \mathcal{G}^F$
$G_i^{s,min}$,$G_i^{s,max}$	min and max capacity (MW) of $i \in \mathcal{G}^S$
$\Delta G_i^{b,max}$,$\Delta G_i^{b,min}$	up- and down-ramping limits of $i \in \mathcal{G}^B$
$\Delta G_i^{f,max}$,$\Delta G_i^{f,min}$	up- and down-ramping limits of $i \in \mathcal{G}^F$
$\Delta G_i^{s,max}$,$\Delta G_i^{s,min}$	up- and down-ramping limits of $i \in \mathcal{G}^S$.

Decision Variables:

x^b_{ti}	base-load generation (MW) at $i \in \mathcal{G}^B$
x^f_{tni}	following reserve generation (MW) at $i \in \mathcal{G}^F$
x^s_{ti}	up-front dispatch (MW) at $i \in \mathcal{G}^S$
x^{p+}_{ti}	planned regulating-up service (MW) at $i \in \mathcal{G}^S$
x^{p-}_{ti}	planned regulating-down service (MW) at $i \in \mathcal{G}^S$
p_{tnij}	power flow (MW) on line $(i,j) \in \mathcal{L}$
θ_{tni}	voltage angle at $i \in \mathcal{B}$
u^s_{tni}	utilization spinning reserves (MW) $i \in \mathcal{G}^S$
u^r_{tni}	utilization of ramping reserve (MW) $i \in \mathcal{G}^R$
x_t	consolidated first-stage decision vector $(= [(x^b_{ti})_{i\in\mathcal{G}^B}, (x^f_{ti})_{i\in\mathcal{G}^F}, (x^s_{ti})_{i\in\mathcal{G}^S}, (x^p_{ti})_{i\in\mathcal{G}^S}])$
y_t	consolidated second-stage decision vector $(= [(p_{tnij})_{(i,j)\in\mathcal{L}}, (\theta_{tni})_{i\in\mathcal{B}}, (u^s_{tni})_{i\in\mathcal{G}^S}, (u^r_{tni})_{i\in\mathcal{G}^R}])$
s_t	state variable $(= [x_{t-1}, y_{t-1}(\bar{\omega}_{t-1})])$.